Biogeosciences Discuss., 9, 5509–5550, 2012
www.biogeosciences-discuss.net/9/5509/2012/
doi:10.5194/bgd-9-5509-2012

Biogeosciences Discussions

Controlling factors of the OMZ in the Arabian Sea

L. Resplandy[1], M. Lévy[2], L. Bopp[1], V. Echevin[2], S. Pous[3], V. V. S. S. Sarma[4], and D. Kumar[4]

[1]Laboratoire des Sciences du Climat et de l'Environnement (LSCE), (CEA, CNRS, UMR8212, UVSQ), IPSL, France
[2]LOCEAN (CNRS, IRD, UPMC, MNHN), IPSL, France
[3]Museum National d'Histoire Naturelle, Paris, France
[4]National Institute of Oceanography, Goa, India

Received: 30 March 2012 – Accepted: 11 April 2012 – Published: 10 May 2012

Correspondence to: L. Resplandy (laure.resplandy@lsce.ipsl.fr)

Published by Copernicus Publications on behalf of the European Geosciences Union.

Abstract

In-situ observations indicate that the Arabian Sea oxygen minimum zone (OMZ) is only weakly influenced by the strong seasonal cycle of ocean dynamic and biogeochemistry forced by the asian monsoon system and it is spatially decorrelated from the coastal upwelling systems where the biological production is the strongest. In this study we examine the factors controlling the seasonality and the spatial distribution of the OMZ in the Arabian Sea using a coupled bio-physical model. We find that the oxygen concentration in the OMZ displays a seasonal cycle with an amplitude of 5–15 % of the annual mean oxygen concentration. The OMZ is ventilated by lateral ventilation along the western boundary current and in the coastal undercurrent along India during the summer monsoon and by coastal downwelling and negative Ekman pumping during the fall intermonsoon and winter monsoon. This ventilation is counterbalanced by strong coastal upwelling and positive Ekman pumping of low oxygen waters at the base of the OMZ during the spring intermonsoon. Although the factors controlling the OMZ seasonality are associated with the men circulation, we find that mesoscale dynamics modulates them by limiting the vertical ventilation during winter and enhancing it through lateral advection during the rest of the year. Processes explaining the establishment and spatial distribution of the OMZ were quantified using a perturbation experiment initialised with no OMZ. As expected, the oxygen depletion is triggered by strong biological activity in central Arabian Sea during winter and in western and eastern boundary coastal upwelling systems during summer. We find that the 3-D ocean dynamic largely controls the spatial distribution of the OMZ. The eastward shift ensues from the northward lateral transport of ventilated waters along the western and eastern coasts and the advection offshore of low oxygen waters formed in the upwelling system.

1 Introduction

Oxygen minimum zones (OMZ) are subsurface oceanic regions where oxygen concentrations reach ultra-low values ($\leq 1\,\mu mol\,l^{-1}$). The most intense OMZs are found in the North and South eastern tropical Pacific, the northwestern Indian Ocean (Arabian Sea) and the eastern tropical Atlantic. The OMZ in the Arabian Sea presents some unique characteristics compared to the other OMZs: it is particularly thick and extends vertically from the bottom of the euphotic layer (~100 m) to ~1000 m and it is not located directly beneath the productive upwelling region (de Sousa et al., 1996; Morrison et al., 1999). This singularity of the Arabian Sea's OMZ is associated with the semi-enclosed geometry of the basin and the monsoonal wind forcing, which result in a unique biannual reversal of the ocean circulation that is not conducive for the development of a typical eastern boundary upwelling system. Instead, the Arabian Sea is characterized by two productive periods associated with the two monsoons (Banse, 1987; Wiggert et al., 2005; Lévy et al., 2007).

During the Northeast Monsoon (NEM, December–February), relatively strong, cool and dry winds blow to the southwest across the Arabian Sea forcing a counterclockwise circulation and inducing a significant ocean heat loss (Fig. 1(1a)). The resulting convective mixing (Bauer et al., 1991; Weller et al., 2002) entrains nutrient-rich waters triggering a phytoplankton bloom north of 15° N (Madhupratap et al., 1996) (Fig. 1(1.b)). During the late stages of the Spring intermonsoon (SIM, March–May) and the Southwest Monsoon (SWM, June–August), the wind and oceanic circulation reverse (Fig. 1(2.a)). The main oceanic features associated with the strong southwesterly wind jet of warm and moist air (referred to as the Findlater Jet, Findlater, 1969) are the coastal upwelling systems that develop along the western (Brock and McClain, 1992; Veldhuis et al., 1997; Hitchcock et al., 2000) and eastern (Banse, 1968; Lierheimer and Banse, 2002) coasts of the Arabian Sea. The strong positive vertical velocities (Fig. 2b and c) upwell nutrients into the euphotic layer enhancing phytoplankton production (Fig. 1(2.b)). These major features of the monsoon periods are modulated

by a strong lateral contrast in Ekman pumping (Fig. 1(1.a) and (2.a)). While NEM winds favor downwelling in the northwest (Fig. 2a) and upwelling in the southwest, the SWM Findlater Jet triggers an open ocean upwelling north of the Findlater Jet (Fig. 2a) and a downwelling to the south (Bauer et al., 1991; Rao et al., 1989; Schott and McCreary, 2001; Fischer et al., 2002; Weller et al., 2002). During the Spring and Fall intermonsoons (FIM, September–November respectively) winds and ocean currents are reversing and much weaker.

While there is considerable seasonal variability in ocean dynamics and biological activity (Barber et al., 2001), no dramatic seasonality has been observed in oxygen concentrations within the OMZ in the Arabian Sea (Fig. 1(1.d) and (2.d)). In the eastern Arabian Sea, a weak intensification of the OMZ during the NEM monsoon has been described (de Sousa et al., 1996), whereas in the western Arabian Sea no significant variability has been observed (Morrison et al., 1999). Various hypotheses were put forward to explain the relative steadyness of the OMZ on the seasonal time-scale. It was first thought that the advection of waters into the Arabian Sea's OMZ was slow which limited the variations in oxygen levels (Severdrup et al., 1942). Later, the maintenance of low oxygen concentrations was attributed to high organic matter decomposition rates that counterbalanced the high levels of local productivity (Ryther and Menzel, 1965) But these initial hypotheses were refuted by Olson et al. (1993) who argued that the residence time in the OMZ (~10 yr) did not support the slow advection hypothesis and that observations of surface productivity, while high, preclude an exceptional high consumption rate at depth. More recently, Sarma (2002) suggested that the absence of seasonality in the OMZ resulted from a the compensation between the physical ventilation of the OMZ and the biological comsumption of oxygen at the seasonal time-scale. In this view, during monsoons the active organic matter remineralisation compensates the large oxygen transport, whilst during intermonsoons the remineralisation of the residual organic matter from the monsoonal blooms is sufficient to compensate the low oxygen transport. This hypothesis could not be verified given the absence of reliable seasonal estimates of oxygen consumption (Sarma, 2002).

Although the spatial offset between the core of the OMZ – located in the northeast Arabian Sea – and the main productive region – located along the western coasts – (Fig. 1(2.b) and (2.d)) has been previously described (Naqvi et al., 2006), very little is known on the biological and physical drivers explaining this singular spatial distribution. Understanding these factors controlling the establishment and spatial distribution of the OMZ is of primary importance when considering its impact on climate and ecosystems. Indeed, the oxygen minimum zone is characterised by an intense denitrification process, which is a key player in the nitrogen and carbon budgets (Codispoti et al., 2001; Naqvi et al., 2006). Denitrification in the Arabian Sea produces about 20 % of the oceanic N_2O, which is a major greenhouse gas (Naqvi et al., 1998). Denitrification is also the most important pathway of losses of fixed nitrogen, which could impact the atmospheric CO_2 sequestration through limitation of total primary production (Falkowski, 1997). In addition, the respiratory barrier of OMZs largely influences the ecosystems structure and is critical for sustaining marine and more particularly commercial species (Levin et al., 2009; Diaz and Rosenberg, 2008).

The two issues of the seasonality and the establishment of the OMZ are addressed in this study with a coupled bio-physical model of the northern Indian Ocean with an explicit representation of the nitrogen and oxygen cycles (Resplandy et al., 2011). This paper is structured as follows. The model setting and the method to derive the oxygen budget are presented in Sect. 2. Section 3 describes the seasonality of the OMZ in the model and observations and investigates the mechanisms at play using the oxygen budget simulated in the model. Section 4 investigates what processes are involved in the establishment and the spatial offset of the OMZ. Finally, Sect. 5 discusses the main results and gives a synthesis of the physical and biogeochemical factors controlling the OMZ in the Arabian Sea.

2 Model and observations

2.1 Model description

The model domain covers the northern Indian Ocean between 5° S and 27° N and includes both the Bay of Bengal and the Arabian Sea. Only results from the Arabian Sea are presented in this study. The NEMO OGCM (Madec, 2008) is used. The vertical grid has 46 levels increasing from 6 m at the surface to 250 m at depth. Northern, eastern and western boundaries are closed by continental masses. The southern boundary (5° S) is a radiative open boundary (Treguier et al., 2001), constrained with a 150 days time-scale relaxation to the monthly meridional velocities, temperature and salinity of the interannual global 1/4° simulation DRAKKAR025-G70 (Barnier et al., 2006). The straits of Bab el Mandeb, Hormuz and Malacca are closed and damped in temperature and salinity toward the Levitus climatology (Levitus et al., 1998) with a 10 days time scale. The initial state is at rest. Temperature and salinity are initialized with the Levitus climatology. The model is forced with the interannual hybrid DRAKKAR Forcing Set 4 (DFS4) extensively described in Brodeau et al. (2009). Momentum, temperature and salinity are advected using a third order diffusive Upstream-Biased Scheme (Shchepetkin and McWilliams, 2005; Madec, 2008), which ensures the model stability in the highly energetic western boundary current without using excessive momentum dissipation. Vertical mixing is modelled with a prognostic turbulent kinetic energy scheme, with background vertical diffusion and viscosity of $10^{-5}\,m^2\,s^{-1}$ and $10^{-4}\,m^2\,s^{-1}$, respectively (Blanke and Delecluse, 1993; Madec, 2008).

The AS covers inshore nutrient-rich habitats where large size-classes phytoplankton such as diatoms dominate and more oligotrophic regions where small size-classes phytoplankton such as dinoflagelates dominate (Banse, 1994; Garrison et al., 1998). In order to account for this diversity, we used the intermediate complexity biogeochemical model Pelagic Interaction Scheme for Carbon and Ecosystem Studies (PISCES) that includes two phytoplankton size-classes corresponding to diatoms and nanophytoplankton and two zooplankton size-classes (Aumont et al., 2003; Aumont and Bopp,

2006). The original version of PISCES was simplified from 24 to 16 tracers, taking out compartments related to the cycling of phosphate and iron, which are not the major limiting nutrients in the Arabian Sea (Aumont et al., 2003; Moore et al., 2004; Dutkiewicz et al., 2005; Koné et al., 2009).

Dissolved oxygen is a prognostic variable in PISCES computed with the following equation:

$$\left(\frac{\partial O_2}{\partial t}\right)_{Bio} = \underbrace{(R^1_{o:c} + R^2_{o:c})(\mu^P_{no3}P + \mu^D_{no3}D)}_{\text{New Production}} + \underbrace{R^1_{o:c}(\mu^P_{nh4}P + \mu^D_{nh4}D)}_{\text{Regenerated Production}} \quad (1)$$

$$- \underbrace{\lambda^\star_{DOC} f(O_2)DOC}_{\text{Remineralisation}} - \underbrace{G^Z Z - G^M M}_{\text{Respiration}} - \underbrace{R^2_{o:c}\text{Nitrif}}_{\text{Nitrification}}$$

Oxygen is produced during photosynthesis (new and regenerated production) by nanophytoplankton (P) and diatoms (D) and consumed by organic matter remineralisation, small (Z) and large (M) zooplankton respiration and nitrification. Nitrif is the conversion of ammonium into nitrate and is assumed to be photoinhibited and reduced in suboxic waters. It is therefore a function of the ammonium and oxygen concentrations and photosynthetically available radiation. In this formulation, stoichiometric ratios account for the change in oxygen relative to carbon during ammonium conversion into organic matter ($R^1_{o:c}$) and during nitrification ($R^2_{o:c}$). Their values have been set respectively to 140:122 and 32:122 so their sum equals the ratio for photosynthesis using nitrate proposed by Takahashi et al. (1985). The consumption of oxygen by remineralisation is weighted by the local oxygen concentration through the function $f(O_2) = (1 - \min\left(1,\ 0.4\frac{\max(0,6-O_2)}{O_2^{min}+O_2}\right))$. When waters become suboxic ($\Delta(O_2) > 0$) nitrate is consumed instead of oxygen (denitrification). Implicitly, degradation rates for respiration and denitrification are therefore identical.

The initial distribution and the southern open boundary conditions for nitrate and oxygen were provided by the global monthly climatology derived from the 50 yr 1/2°

simulation of Koné et al. (2009), which was in turn initialized with the World Ocean Atlas 2005. The other biological tracers were initially set to low values. Nitrogen and silicate supplies by rivers are derived from the same model using constant N/Si/C ratios (Koné et al., 2009). As for temperature and salinity, nitrate and oxygen were damped in the Bab el Mandeb, Hormuz and Malacca straits. To ensure positive values, biogeochemical tracers are advected with the positive Monotone Upstream-centered Schemes for Conservation Laws (Van Leer, 1979; Lévy et al., 2001) and dissipated along isopycnals at small scales by a laplacian operator with a diffusion coefficient of 100 $m^2\,s^{-1}$. Biogeochemical model formulations and parameters are summarized in the Appendix of Resplandy et al. (2011).

2.2 Model experiments

The eddy-resolving simulation of Resplandy et al. (2011) is used to study the seasonal variability of the OMZ in the Arabian Sea. In this experiment the horizontal resolution is of 1/12° (~9 km). This resolution enables to capture mesoscale processes which improves the representation of the two seasonal blooms (1) by vertical advection of nutrients in the early stage of upwelling and by efficient offshore transport of nutrients into the central Arabian Sea during the summer monsoon and (2) by mesoscale vertical advection of nutrients in the central Arabian Sea during the winter monsoon. The model was integrated from 1992 to 2003 and a climatology was built by averaging from 1995 to 2003. The model ability at simulating the seasonal cycle of circulation, mixed layer depth, nutrients concentrations and phytoplankton was evaluated in Resplandy et al. (2011). Section 3 examines the seasonal cycle of the oxygen budget based on this same climatology.

In order to examine the establishment of the OMZ, a longer perturbation experiment was carried in which the long-term evolution of oxygen is examined. In this experiment, the oxygen initial distribution is modified: all concentrations below 100 µmol l^{-1} are set to 100 µmol l^{-1} and all concentrations above 100 µmol l^{-1} are kept unchanged. This experiment was performed with a 1/4° horizontal resolution (which decreases the

computation costs by ∼30 compared to the 1/12°). This sensitivity experiment was run for 33 yr. Note that a zone of reduced oxygen concentrations (<80 µmol l^{-1}) was generated after 33 yr, which is not as intense as the OMZ in observations. This experiment is however suited to the examination of the mechanisms controlling the formation of the OMZ.

2.3 Oxygen budget

The oxygen concentration in the model evolves according to:

$$\partial_t O_2 = \underbrace{\left(\frac{\partial O_2}{\partial t}\right)_{\text{Dyn}}}_{\text{Dynamical transport}} + \underbrace{\left(\frac{\partial O_2}{\partial t}\right)_{\text{Bio}}}_{\text{Biological sources and sinks}} + J_{\text{flux}} \quad (2)$$

$\left(\frac{\partial O_2}{\partial t}\right)_{\text{Bio}}$ denotes all biological processes affecting the concentration of O_2, which includes production by photosynthesis and consumption by remineralization, zooplankton respiration and nitrification (see Eq. 1). The dynamical transport of oxygen $\left(\frac{\partial O_2}{\partial t}\right)_{\text{Dyn}}$ follows:

$$\left(\frac{\partial O_2}{\partial t}\right)_{\text{Dyn}} = - \underbrace{u_H.\nabla_H O_2}_{\text{lateral advection}} - \underbrace{u_Z.\nabla_Z O_2}_{\text{vertical advection}} + \underbrace{\frac{\partial K_z \partial O_2}{\partial z^2}}_{\text{vertical mixing}} \quad (3)$$

Finally, J_{flux} is the flux of O_2 from air to sea (F_{O_2}) divided by the depth of the surface layer. F_{O_2} is calculated from:

$$F_{O_2} = k_w(\alpha O_{2\text{atm}} - O_2) \quad (4)$$

where k_w is the transfer velocity, ($\alpha O_{2\text{atm}} - O_2$) is the difference in O_2 partial pressure between the air and surface sea water and α the solubility of O_2 in seawater.

The various terms $\left(\frac{\partial O_2}{\partial t}\right)_{\text{Bio}}$ and $\left(\frac{\partial O_2}{\partial t}\right)_{\text{Dyn}}$ simulated in the model are examined to estimate the biological and dynamical contribution to the seasonality and the formation of the OMZ in the Arabian Sea. Note that J_{flux} is not presented because it only impacts the surface layer and not the levels were the OMZ is located.

3 OMZ seasonal variability

3.1 OMZ in model and observations

The model physical solution and the simulated phytoplankton, nutrients and primary production have been evaluated in detail in Resplandy et al. (2011). Here we examine how the OMZ and its seasonality in the model compare to the World Ocean Atlas 2009 (WOA09) seasonal climatology. The core of the OMZ (defined as $O_2 \leq 20$ µmol l^{-1} following Paulmier and Ruiz-Pino, 2009) is confined to the enclosed part of the basin north of 10° N and roughly spreads vertically between 200 and 1000 m (Fig. 1d and Fig. 3a, c). The OMZ presents a east-west contrast with lower oxygen concentrations at the center of the basin and higher concentrations along the coasts, in particular along the Omani coast (Fig. 1d and Fig. 3a). The OMZ is reproduced by the model but oxygen concentrations are slightly larger than observed just below the euphotic layer (∼100 m depth) and along the western coast inducing a reduction of the core's volume (Fig. 1d, e and Fig. 3). This bias primarily arises from the relatively low vertical resolution in the model (46 vertical levels with 10 levels between 50 and 300 m) that is insufficient to properly resolve the sharp oxygen gradient (Fig. 3). Along the western coast, core waters with oxygen concentrations ≤20 µmol l^{-1}) are observed between 400 and 1000 m, whereas oxygen concentration in the model reach 30 µmol l^{-1} (see contours on Fig. 3a, b).

Seasonal variations of the oxygen concentration appear in the WOA09 climatology despite the relatively low number of observations particularly below 200 m (Fig. 4a,

c): at the top (100 µmol l^{-1} isoline between 100 and 200 m) , in its core (20 µmol l^{-1} isoline between 400 and 800 m) and at its base (100 µmol l^{-1} isoline between 1000 and 2000 m). They can be interpreted qualitatively as a response to the monsoonal change in circulation. The top of the OMZ is uplifted by ∼50–100 m along the western, eastern and northern coasts where upwelling occur during SWM (Fig. 4a, c). The depth of the OMZ's top is also modulated seasonally in the central Arabian Sea. The 100 µmol l^{-1} isoline is doming in the southeast (south of 15° N and east of 65° E, Fig. 4a and c) and deepening in the northwest (north of 20° N and west of 60° E, Fig. 4a and c) during the NEM, while the opposite is observed during the SWM. This northwest-southeast contrast in the depth of the OMZ's top is most likely related to the lateral variations in Ekman pumping forced on either side of the dominant monsoonal wind (Fig. 1a). The core of the OMZ is also impacted by the eastern and northern coastal upwelling and by Ekman pumping in the central Arabian Sea by the northward western boundary current (Fig. 4a, c). In addition, a strong reduction of the OMZ vertical extension is observed along the western coast (between 200 and 500 m) during the SWM (Fig. 4a). This increase in oxygen concentration is most likely related to the advection of southern waters into the Arabian Sea (Fig. 1(2.a)). Finally, at depth, the 100 µmol l^{-1} isoline is globally uplifted during the SWM when compared to the NEM (Fig. 4a, c).

These seasonal changes associated with upwelling, Ekman pumping and lateral advection by the western boundary current are reproduced in the model (Fig. 4b, d). However, the two model biases described previously also affect the representation of the seasonal variability: the weaker subsurface oxygen gradient in the model results in a weaker uplift of the top of the OMZ in regions of coastal upwelling and positive Ekman pumping (Fig. 4b, d); the reduction of the core along the western coast during the SWM is represented in the model but is too intense when compared to observations (Fig. 4b). In the following, we further examine the processes explaining the seasonal changes in the OMZ by quantifying the dynamical and biological terms of the oxygen budget in the model (Eq. 2).

3.2 Oxygen budget in OMZ

The oxygen concentration in the AS region (52–77° E, 12–26° N, 200–1500 m, defined on Fig. 1(2.e)) displays a seasonal cycle that roughly peaks during the SWM and NEM periods (black contours on Fig. 5a and Sect. 3.1). Here we examine this seasonality by quantifying the seasonality of the biological and dynamical trends in the O_2 equation (Eqs. 1 and 3). As expected biological consumption is confined to the upper 300 m and is maximal during the productive NEM and SWM periods (Fig. 5b). During these monsoon periods, the dynamical trend counteracts the biological uptake by ventilating the upper 400 m (Fig. 5c), which is in agreement with the results of Sarma (2002). However, the amplitude of the dynamical trend in our model is by far larger than the biological contribution, which does not support the hypothesis of Sarma (2002) of a compensation between the ventilation and biological uptake of oxygen at the seasonal time-scale. In the model, the excess of oxygen brought to upper part of the OMZ during the SWM, FIM and NEM periods is then compensated by the input of comparatively low-oxygenated waters during the SIM period (Fig. 5). The resulting seasonality is most intense in the upper OMZ, where it represents 15 % of the total oxygen concentration (amplitude of annual variations of ∼6 µmol l^{-1} for an annual mean oxygen concentration of 40 µmol l^{-1}, Fig. 5a). In the lower part of the OMZ and in the core the seasonality is lower and of order the of 5 % (amplitude of annual variations of ∼1–3 µmol l^{-1} for an annual mean oxygen concentration of 20–40 µmol l^{-1}, Fig. 5a).

This oxygen budget averaged over the AS region reflects the mean balance regardless of regional differences. Now, we further investigate the impact of the dynamical transport by focusing on three contrasted regions (defined on Fig. 1(2.e)): a region of the central Arabian Sea where the OMZ's core is most intense (noted CAS) and two coastal regions under the influence of the upwelling systems of Oman (noted OMA) and India (noted IND) respectively. The oxygen budget in these three key regions confirms that the dynamical transport is the main driver of the seasonality in the OMZ (Fig. 6a

and b). Only the contributions of vertical and horizontal advection are presented here, vertical mixing being much smaller below 200 m.

In the CAS region, the top of the core is ventilated during the during the FIM and NEM periods and deoxygenated during the late SIM and SWM (Fig. 6(1.c)). The seasonal changes at the base of the core are roughly anti-correlated to those simulated at the top. This seasonality primarily arises from the vertical advection of oxygen associated with Ekman pumping. During the FIM and NEM periods, negative vertical velocities transport surface ventilated waters into the top of the OMZ and deepen the core of the OMZ (Fig. 2a and Fig. 6(1.c)). During the late SIM and SWM periods positive Ekman pumping upwells the OMZ resulting in reduced oxygen concentration at the top of the OMZ and enhanced concentrations at its base (Fig. 2a and Fig. 6(1.c)). The contribution of horizontal advection in CAS is confined to the upper boundary of the OMZ (200–300 m, Fig. 6(1.d)). The top of the OMZ is ventilated horizontally between the NEM and the SWM periods (December–August) by a southeastward transport related to the advection of waters originating from the Red Sea during the NEM and SIM and from the upwelling of Oman during the SWM.

The oxygen budget in OMA is largely influenced by the dynamical signature of the coastal upwelling system that is active during the late-SIM and SWM periods (Fig. 6(2)). The impact of the summer intense coastal upwelling (occurring between May and July) is counterbalanced by downwelling during the rest of the year (Fig. 2b). Vertical advection associated with the upwelling system upwells the core of the OMZ leading to a substantial decrease of oxygen concentrations at the top of the OMZ and an input of waters with comparatively higher oxygen concentration at its base (Fig. 6(2.c)). The impact of vertical advection associated with the coastal upwelling is largely modulated by lateral advection. During SIM and SWM periods, OMA and more generally the western coast of the Arabian Sea is ventilated by the intense western boundary current or Somali Current (SC on Fig. 1(2.a)) that transports oxygenated waters northward (Fig. 6(2.d)). During the FIM and NEM periods, the circulation reverses and low oxygen waters originated from the OMZ's core are transported into OMA (Fig. 1(1.a)). Although

the advection of oxygen extends down to 800 m in both season, the coastal current's intensity and thus the impact on the oxygen budget are much larger during the SIM and SWM periods (Fig. 6(2.d)).

Although the IND region is also under the influence of a seasonal coastal upwelling (Fig. 1(2.a) and Fig. 2b), the oxygen budget is very different from the one in the OMA region (Figs. 6(2 and 3)). Unlike the other areas, the IND region is under the influence of a semi-annual (~180 days) seasonal cycle (Fig. 2). This semi-annual forcing results in positive vertical velocities in April–June when the coastal upwelling occurs but also in November–January and negative vertical velocities in February–March and July–September. This semi-annual forcing arises from the interactions of second-baroclinic-mode Kelvin and Rossby waves that strongly influences the sea level variability (Han et al., 2011) and therefore the vertical transport along the west coast of India. The OMZ in IND is also influenced by the lateral transport of oxygen by the undercurrent that spreads below 150 m depth (Fig. 6(3.d), Shetye et al., 1990). During the SIM and SWM, this northward undercurrent transports ventilated waters into the Arabian Sea. During the FIM and NEM the circulation reverses and the undercurrent transports low oxygen waters originated from the OMZ southward into the IND region. Note that whereas the OMZ in OMA is under the influence of the strong western boundary current that extends from the surface down to 800 m, the OMZ in IND is not largely impacted by the current system confined to the surface but by the subsurface circulation.

3.3 Impact of mesoscale

The relative importance of the mean circulation and eddy-driven processes on the seasonal changes in oxygen concentration is estimated using the Reynold's decomposition. Following this method, lateral and vertical advective supply of oxygen can be

separated into:

$$\underbrace{\overline{(-u_H.\nabla_H O_2)}}_{\text{total lateral advection}} = \underbrace{\overline{(-u_H}\cdot\overline{\nabla_H O_2)}}_{\text{mean lateral flow}} + \underbrace{\overline{(-u'_H\cdot\nabla_H O'_2)}}_{\text{eddy lateral flow}} \quad (5)$$

$$\underbrace{\overline{(-w.\nabla_Z O_2)}}_{\text{total vertical advection}} = \underbrace{\overline{(-w}\cdot\overline{\nabla_Z O_2)}}_{\text{mean vertical flow}} + \underbrace{\overline{(-w'\cdot\nabla_Z O'_2)}}_{\text{eddy vertical flow}} \quad (6)$$

where the over-bar denotes a time mean to be defined and the prime all deviations from this time mean (referred as the eddy term). To exclude the contribution of seasonal variations from the eddy term and incorporate them into the mean term, we defined the mean state of $\overline{u_H}$, $\overline{w}$ and $\overline{O_2}$ as the monthly, ten-year mean climatology of u_H, w and O_2.

The comparison of the mean and eddy contributions over the AS region suggests that most of the seasonality simulated in the OMZ can be attributed to the mean circulation (Fig. 7). This strengthens our previous finding highlighting the major role of Ekman pumping and coastal upwelling and downwelling in modulating the oxygen concentration in the OMZ at the seasonal time-scale. In average over the AS, eddies contribution to the oxygen budget in the OMZ is of the order of ∼10 % and results in the ventilation of the OMZ (Fig. 7b). At the top of the OMZ, the eddy-driven ventilation is mostly associated with the vertical advection of surface ventilated waters during the SIM and SWM and with horizontal advection during the FIM and NEM periods (Fig. 7c and d). At the base of the OMZ, the dominant effect of mesoscale is the weak vertical advection of deep and comparatively oxygen-rich waters into the OMZ.

4 OMZ formation

In all OMZ of the world's ocean but the OMZ of the Arabian sea, the OMZ is found just below very productive upwelling systems and the presence of the OMZ is explained essentially be 1D processes: it is the consequence of the degradation at depth of the

organic material produced at the surface. In the case of the Arabian sea, the OMZ is not found below the area of strongest productivity in the upwelling of Oman. Rather, the OMW is shifted toward the center of the Arabian Sea. This suggests that lateral advection processes play a role in this shift.

However, in a system close to equilibrium, such as the model experiment that we have used previously, this shift cannot be explained. Indeed, at equilibrium, $\overline{\frac{\partial O_2}{\partial t}}$ is zero (where the overbar is a long term average), which means that the biological term and dynamical term are in balance ($\overline{\left(\frac{\partial O_2}{\partial t}\right)_{\text{Bio}}} = -\overline{\left(\frac{\partial O_2}{\partial t}\right)_{\text{Dyn}}}$, see Sect. 2.3). As shown in Fig. 5, in our model run, the biological and dynamical trends are both maximum on the western side of the AS, where they tend to balance each other: thus this balance is not sufficient to explain the shift in the OMZ location. We can also note that the two terms are not in perfect balance, mostly because of the presence of internal variability (the signature of eddies is still apparent on the long term mean of the dynamical trend), of interannual variability, and of the model drift.

To overcome this issue, it is useful to perturb the system and see how it goes back to equilibrium. In a perturbed experiment, $\overline{\frac{\partial O_2}{\partial t}}$ is different from zero and its structure gives insights on why and where the OMZ is established. In the following, we have conducted such a perturbed experiment by filling in the OMZ: all oxygen concentrations $\leq$100 µmol l^{-1} were arbitrary set to 100 µmol l^{-1} in the initial oxygen field. Moreover, the relatively low impact of mesoscale found in the previous section allowed us to use an eddy-permitting model (1/4°) which permitted to conduct a longer experiment (33 yr).

During the perturbation experiment, the oxygen concentration between 200 and 1500 m rapidly evolves (Fig. 9). Oxygen consumption is most intense in the northwest and expands gradually to the southeast of the Arabian Sea. A second region of low oxygen concentrations appears along the south Indian coast and superimposes to the oxygen depletion from northwest origin (Fig. 9). In average over the AS region, the oxygen concentration between 200 and 1500 m drastically departs from the concentration

of the initial state (between 100 and 120 µmol l^{-1}). After 5 to 10 yr, waters with concentrations between 80 and 100 µmol l^{-1} are formed and after 15 yr, waters with concentration lower than 80 µmol l^{-1} appear (Fig. 10). At the end of the simulation, waters of concentrations lower than 80 µmol l^{-1} represent about 20 % of the total water mass.

Although a much longer integration time would be necessary to reproduce the magnitude of the observed OMZ's, the model generates a region of reduced oxygen spatially consistent with observations. In addition, the spatial distribution of the simulated oxygen trend at the end of the perturbation experiment, i.e. the sum of biological and dynamical processes influencing oxygen concentration, is very similar to the observed distribution of the OMZ (Fig. 11(3.a) and Fig. 1d). The physical and biological processes at play in the OMZ's formation are discussed below. A global view of the processes shaping the OMZ in the Arabian Sea is given by averaging the trends vertically (between 200 and 1500 m) and during three periods of time corresponding to three periods of the simulation (Fig. 11): the beginning (years 1 to 5), the end (years 29 to 33) and an intermediate period (years 14 to 19).

At the beginning of the simulation, oxygen is largely consumed by biological processes over the whole Arabian Sea and more particularly in regions of seasonal blooms (Fig. 11(1.b)). This consumption is most intense along the western and northern coasts of the Arabian Sea, which corresponds respectively to the upwelling system of Oman that is productive during the SWM and the northern Arabian Sea that is productive during the NEM (Fig. 11b). Oxygen consumption is also relatively large in the southeast Arabian Sea, where the upwelling system of India onsets during the SWM (Fig. 11b). During the first five years of simulation the dynamical contribution to the oxygen budget is small (Fig. 11(1.c)). Oxygen concentrations are indeed relatively homogeneous (black contours on Fig. 11(1)) and the impact of advection is therefore minor (Fig. 11(1.c)). The balance between the biological consumption and the dynamical transport results in a strong drawdown of the oxygen concentration (Fig. 11(1.a)). The biological consumption is relatively steady through the simulation with a slight decrease of remineralisation and respiration in response to the decreasing oxygen concentration

(Fig. 11b). In contrast, the dynamical transport of oxygen becomes stronger as the oxygen drawdown located in biologically active regions enhances horizontal and vertical oxygen gradients (Fig. 11c). The advection redistributes the oxygen within the basin by ventilating the western coast and in a lesser extent the eastern coast of the Arabian Sea and by transporting low oxygen waters from the coasts to the central eastern Arabian Sea (Fig. 11(3.c)). Toward the end of the simulation, the balance between the biological consumption and the dynamical transport clearly indicates that the region of highest oxygen drawdown is located in the central eastern Arabian Sea where the actual observed OMZ is located (Fig. 11(3.a) and Fig. 1(1.d)). The oxygen minimum formed during the 33 yr of simulation presented here can be interpreted as a proto-OMZ. Eventually, over a longer period of time, the dynamical term would increase until it equals the biological term at each grid point and the OMZ formed prior to this equilibrium would be maintained.

5 Discussion

5.1 Seasonality in the OMZ

The simulated OMZ extends between 100 and 2000 m and its core (≤20 µmol l^{-1}) is located between 200 and 1000 m, which is similar to the observed climatology. The seasonality detected in observation is weak and the scarcity of observations makes it difficult to assess if it is associated with the seasonality rather than with the low spatio-temporal sampling. However, the good agreement between the changes in oxygen concentration in observations and the in model gives us confidence that the OMZ responds to the monsoonal seasonality (Fig. 4). The model predicts a seasonality in oxygen concentrations, which has an amplitude of ∼15 % of the annual mean concentration in the upper part of the OMZ and of 5 % in the core.

The seasonality in the model results from unbalanced budget between oxygen physical transport and biological consumption. The biological uptake of oxygen is most

intense in the upper 300 m during the winter and summer monsoons. Its contribution to the simulated oxygen budget within the OMZ is 3 to 5 times lower than the physical transport (Fig. 5). The model predicts a compensation of oxygen trends between the upper and lower OMZ . However, the signature in the upper OMZ prevails on the seasonal cycle of oxygen, the seasonality being most intense in the upper part (Figs. 5 and 6). On average over the basin as well as on the regional scale, the strong seasonality in the factors controlling the oxygen concentration and the unbalance between the biological and dynamical processes do not support the hypothesis of a compensation between physical ventilation and remineralisation that has been put forward to explain the maintenance of the OMZ (Sarma, 2002).

The upper OMZ is ventilated during summer, fall and winter, which is then compensated by the input of low oxygen waters during spring. In summer, the ventilation is mostly sustained by the lateral transport of southern waters in the western boundary current and by their transport offshore into the central Arabian Sea. This result is supported by observed oxygen transects that show a ventilation of the OMZ's core along the western coast during summer (Fig. 4). Another source of oxygen in the model is related to the input of Red Sea waters in the northern Arabian Sea. During fall and winter, the OMZ is ventilated by coastal downwelling along the northern, eastern and western coasts and negative Ekman pumping in the northwestern central Arabian Sea. This result is also supported by observations that highlight this downwelling along the eastern, western and northern coasts and a deepening of the OMZ's top in the central Arabian Sea (Fig. 4). During spring, deep waters are brought into the OMZ by positive Ekman pumping in the central Arabian Sea and coastal upwelling in particular along Oman and India thus counterbalancing the ventilation by surface waters occurring the rest of the year. Note that coastal and open-ocean upwelling are still active during the summer monsoon but their impact is counterbalanced by lateral ventilation. The lower OMZ is mostly under the influence of upwelling and downwelling (coastal and Ekman), whose effect at depth are opposed to the effect at the surface (Figs. 5 and 6). In addition, the

undercurrent along the coast of India transport oxygen into the Arabian Sea from late winter to the end of summer (Fig. 6(3.d)) .

One of the regions of greatest variability in our model is the upwelling system along the Indian coast (Fig. 6). Unlike in the rest of the Arabian Sea where the seasonality of the OMZ is annual (365 days), the OMZ in this area is subjected to a semi-annual forcing (~180 days). Indeed, oxygen concentrations are influenced by the propagation of coastal Kelvin waves and westward propagating Rossby waves (Figs. 2 and 6). The combination of this semi-annual forcing and the ventilation by the undercurrent from late winter to summer results in lower oxygen concentration during the winter monsoon. This is rather surprising as one would expect oxygen concentration to be lower when coastal upwelling favors biological activity and upwells low-oxygenated waters. However, this results is in very good agreement with oxygen observations sampled during three cruises in winter, spring and summer that evidenced a large drawdown of oxygen during winter (de Sousa et al., 1996).

Although the OMZ's seasonality is mostly associated with the mean circulation, the mechanisms at play are modulated by the mesoscale circulation. In average mesoscale structures tend to ventilate the OMZ (Fig. 7). During the summer monsoon and the spring and fall intermonsoons, the predominant effect of mesoscale structures is the offshore export of ventilated waters from the upwelling off Oman and India. This eddy-induced offshore transport in the model is most intense in the western boundary upwelling of Oman, where ~100 km width mesoscale filaments extend ~500–1000 km into the central Arabian Sea. Although the major role of these structures in exporting upwelled waters and nutrients offshore is quite well described (Brock et al., 1991; Keen et al., 1997; Brink et al., 1998; Manghnani et al., 1998; Lee et al., 2000; Kawamiya, 2001), their contribution to the oxygen budget was not yet assessed. In contrast, the lateral export of oxygen out of the Indian upwelling is mostly mediated by mesoscale eddies of 50–100 km and the 10–50 km width filaments wrapped around them, which are constant features of eastern boundary upwelling (Batteen, 1997; Leth and Middleton, 2004; Blanke et al., 2005; Capet et al., 2008).

During the winter monsoon, eddy-induced advection tend to decrease the oxygen concentration in the upper OMZ (Fig. 7). At this time of year, numerous mesoscale eddies (∼100 km radius), generated by the propagation of Rossby waves resulting from the Ekman pumping and the northward propagation of coastal Kelvin waves, populate the Arabian Sea north of 12° N (Flagg and Kim, 1998; Kim et al., 2001; Schott and McCreary, 2001; Fischer et al., 2002; Al Saafani et al., 2007). As highlighted in Resplandy et al. (2011), these mesoscale eddies are surrounded by filamentary structures associated with shallow mixed layers (∼50 m) compared to the surrounding values (∼100–120 m). This restratification effect of the mesoscale is related to the presence of density fronts that become unstable as the eddy field is stirred and deformed (Lapeyre et al., 2006; Lévy et al., 2010). The stabilisation of these fronts generates an ageostrophic circulation, which tends to restratify the water column (Lévy et al., 1999; Nurser and Zhang, 2000; Oschlies, 2002). This eddy-induced restratification limits the penetration of surface oxygenated waters into the OMZ that is associated with convective mixing (in the upper 150 m) and relayed deeper in the water column by Ekman vertical advection.

5.2 OMZ spatial distribution

The factors controlling the spatial distribution of the OMZ were examined using a perturbation experiment initialised with no oxygen concentration below 100 µmol l^{-1}. Although a much longer simulation would be necessary to reproduce the intensity and spatial extent of the OMZ, the simulated oxygen budget during the establishment of a low oxygen region reflects the observed eastward shift of the OMZ core compared to the region of highest biological activity. As expected, the biological consumption of oxygen is most active in the northern and western Arabian Sea and in a narrow band along the coast of India, which are the regions where the winter and summer monsoonal blooms occur. As oxygen horizontal gradients are created by the inhomogeneous biological consumption, lateral transport redistributes oxygen within the Arabian Sea. In our model, the spatial shift between the biological consumption of oxygen and the OMZ arises from the lateral ventilation of the two productive regions of coastal upwelling and

by the lateral transport of low oxygen waters from the coasts to the central eastern Arabian Sea.

The advection of waters of high oxygen concentration from the south along the western boundary during summer explains the ventilation along the coasts of the Arabic Peninsula. The impact of this ventilation extends offshore with the intense lateral transport from the upwelling system. As previously described, this western boundary upwelling system is characterised by 100 km wide mesoscale filaments exporting coastal ventilated waters ∼500–1000 km offshore (see Sect. 5.1). Although mesoscale is better represented in the 1/12° horizontal resolution simulation used to study the seasonality, some of these relatively large structures are present in the 1/4° simulation used here. In addition the upwelling region along the coast of India is also ventilated by the undercurrent transporting southern waters into the Arabian Sea also described in the previous section.

The major role of lateral advection along the western boundary and the subsequent mesoscale transport on controlling the eastward shift of the OMZ in the Arabian Sea is in agreement with the study of McCreary et al. (2011) using a different approach. In a suite of experiments, they identify the importance of taking into account the physical transport of oxygenated waters from the south and the additional mixing induced by eddies to properly resolve the OMZ. The possible impact of biological rates such as the remineralisation rate or the particle sinking rate has not been considered in our model study. Some sensitivity experiments realised with another model however show that the detrital sinking rate could influence the depth of the OMZ in the Arabian Sea (McCreary et al., 2011). Indeed, slow detrital sinking rates in the western Arabian Sea could promote the northward and eastward advection of detritus before they are being remineralised. Nevertheless, McCreary et al. (2011) conclude that the choice of biological parameters only weakly influences the representation of the OMZ compared to the physical transport.

A major concern is that OMZs will expand in the future due to global climate change Keeling et al. (2010). Observational evidence indicate that oxygen levels in the ocean

interior have indeed declined over the past 50 yr (Ono et al., 2001; Stramma et al., 2008) and climate models predict a future enhancement of this decline as the upper ocean warms and becomes more stratified (Bopp et al., 2002; Keeling et al., 2010). The threat of future ocean deoxygenation is important, both because of the direct environmental consequences of oxygen changes such as the loss of habitat for high-oxygen-demand species (Stramma et al., 2011), as well as because of the possible implications for greenhouse gases (N_2O and CO_2). However, data on oxygen changes are mostly indicative of the Pacific and Atlantic OMZs and few if any climate model successfully represents the monsoonal circulation in the Arabian Sea. In addition, paleorecords indicate that past changes in oxygen concentration in the Arabian Sea's OMZ differed from the changes inferred in other OMZs (Jaccard and Galbraith, 2012). Whereas oxygen concentrations decreased within the upper 800 m of the eastern tropical Pacific during the last glacial maximum, oxygen concentrations increased in the Arabian Sea in conjunction with a reduction of export production, most likely associated with changes in circulation and upwelling conditions. The present study also suggests that the highly energetic and peculiar 3-D physics associated with the monsoonal reversal, which is a major driver of the present OMZ could be a of primary importance when examining past and future changes.

6 Conclusions

The surprisingly low seasonal signal in oxygen concentration and the spatial offset between coastal upwelling and depleted oxygen levels are two specific characteristics of the Arabian Sea oxygen minimum zone. Using a biophysical model, we identify and quantify the processes regulating the seasonal cycle and the spatial offset of the oxygen minimum zone in the Arabian Sea.

The main results of this study are:

- The seasonality in the model is estimated to be ~5 to 15 % of the annual mean oxygen concentration. Despite their low spatio-temporal coverage, observations support the existence of such a weak seasonality.
- The seasonality is mainly driven by the input of ventilated surface waters during fall, winter and summer and the input of low oxygen concentration during spring.
- During fall and winter, the major processes ventilating the OMZ are coastal downwelling and negative Ekman pumping in the central Arabian Sea.
- During spring, upwelling along the western, eastern and northern coasts and positive Ekman pumping upwell the OMZ replacing ventilated surface waters by deeper waters of comparatively lower oxygen concentration.
- During summer, lateral ventilation along the western boundary current and in the coastal undercurrent along India largely counterbalance the effect of coastal and Ekman upwelling that onset during spring.
- Mesoscale processes slightly modulate the oxygen budget by limiting the vertical ventilation during winter and enhancing it through lateral advection during the rest of the year.
- The spatial shift between the OMZ and the region of high productivity associated with coastal upwelling arises from the lateral advection of southern ventilated waters along the western coast and in a lesser extent along the eastern coast and the transport offshore of low oxygen waters originated from the upwelling systems into the central Arabian Sea.

Acknowledgements. We sincerely thank the NEMO system team for their development and maintenance of the NEMO ocean general circulation model. Support was provided by the TANGGO (Toward AN Eddying Global Green Ocean) and Carbochange programs. The Chl data were provided by the SeaWiFS Project and NASA's DAAC.

The publication of this article is financed by CNRS-INSU.

References

Al Saafani, M. A., Shenoi, S. S. C., Shankar, D., Aparna, M., Kurian, J., Durand, F., and Vinayachandran, P.: Westward movement of eddies into the Gulf of Aden from the Arabian Sea, J. Geophys. Res., 112, C11004, doi:10.1029/2006JC004020, 2007. 5529

Aumont, O. and Bopp, L.: Globalizing results from ocean in situ iron fertilization studies, Global Biogeochem. Cy., 20, GB2017, doi:10.1029/2005GB002591, 2006. 5514

Aumont, O., Maier-Reimer, E., Blain, S., and Monfray, P.: An ecosystem model of the global ocean including Fe, Si, P colimitations, Global Biogeochem. Cy., 17, GB1060, doi:10.1029/2001GB001745, 2003. 5514, 5515

Banse, K.: Hydrography of the Arabian Sea Shelf of India and Pakistan and effects on demersal fishes, Deep Sea Research and Oceanographic Abstracts, 15, 45–48, IN7–IN10, 49–79, doi:10.1016/0011-7471(68)90028-4, 1968. 5511

Banse, K.: Seasonality of phytoplankton chlorophyll in the central and northern Arabian Sea, Deep Sea Res. I, 34, 713–723, doi:10.1016/0198-0149(87)90032-X, 1987. 5511

Banse, K.: On the coupling of hydrography, phytoplankton, zooplankton, and settling organic particles offshore in the Arabian Sea, Proceedings of Indian Academy Sciences (Earth and Planetary Sciences), 103, 125–161, 1994. 5514

Barber, R. T., Marra, J., Bidigare, R. C., Codispoti, L. A., Halpern, D., Johnson, Z., Latasa, M., Goericke, R., and Smith, S. L.: Primary productivity and its regulation in the Arabian Sea during 1995, Deep Sea Res. II, 48, 1127–1172, doi:10.1016/S0967-0645(00)00134-X, 2001. 5512

Barnier, B., Madec, G., Penduff, T., Molines, J., Treguier, A., Sommer, J. L., Beckmann, A., Biastoch, A., Boning, C., Dengg, J., Derval, C., Durand, E., Gulev, S., Remy, E., Talandier,

C., Theetten, S., Maltrud, M., McClean, J., and Cuevas, B. D.: Impact of partial steps and momentum advection schemes in a global ocean circulation model at eddy permitting resolution, Ocean Dynam., 56, 543–567, doi:10.1007/s10236-006-0082-1, 2006. 5514

Batteen, M. L.: Wind-forced modeling studies of currents, me- anders and eddies in the California Current System, J. Geophys. Res., 28, 2199–2221, 1997. 5528

Bauer, S., Hitchcock, G. L., and Olson, D. B.: Influence of monsoonally-forced Ekman dynamics upon the surface-layer depth and plankton biomass distribution in the Arabian Sea, Deep-Sea Res., 38, 531–553, 1991. 5511, 5512

Blanke, B. and Delecluse, P.: Variability of the tropical atlantic ocean simulated by a general circulation model with two different mixed-layer physics, J. Phys. Oceanogr., 23, 1363–1388, 1993. 5514

Blanke, B., Speich, S., Bentamy, A., Roy, C., and Sow, B.: Modeling the structure and variability of the southern Benguela upwelling using QuikSCAT wind forcing, J. Geophys. Res., 110, C07018, doi:10.1029/2004JC002529, 2005. 5528

Bopp, L., Quéré, C. L., Heimann, M., Manning, A. C., and Monfray, P.: Climate-induced oceanic oxygen fluxes: Implications for the contemporary carbon budget, Global Biogeochem. Cy., 16, 1022, doi:10.1029/2001GB001445, 2002. 5531

Brink, K., Arnone, R., Coble, P., Flagg, C., Jones, B., Kindle, J., Lee, C., and Phinney, D.: Monsoons boost biological productivity in Arabian Sea, Eos Trans. AGU, 79, 165, 1998. 5528

Brock, J. C. and McClain, C. R.: Interannual Variability in Phytoplankton Blooms Observed in the Northwestern Arabian Sea During the Southwest Monsoon, J. Geophys. Res., 97, 733–750, 1992. 5511

Brock, J. C., McClain, C. R., Luther, M. E., and Hay, W. W.: The phytoplankton bloom in the northwestern Arabian Sea during the Southwest Monsoon of 1979, J. Geophys. Res., 96, 20623–20642, 1991. 5528

Brodeau, L., Barnier, B., Penduff, T., Tréguier, A.-M., and Gulev, S.: An ERA40 based atmospheric forcing for global ocean circulation models, Ocean Modell., 31, 88–104, doi:10.1016/j.ocemod.2009.10.005, 2009. 5514

Capet, X., Colas, F., McWilliams, J. C., Penven, P., and Marchesiello, P.: Eddies in eastern boundary subtropical upwelling systems, in Ocean Modeling in an Eddying Regime, Geophys. Monogr. Ser., vol. 177, edited by: Hecht, M. W. and Hasumi, H., 131–147, AGU, Washington, DC, doi:10.1029/177GM10, 2008. 5528

Codispoti, L. A., Brandes, J. A., Christensen, J. P., Devol, A. H., Naqvi, S. W. A., Paerl, Paerl, H. W., and Yoshinari, T.: The oceanic fixed nitrogen and nitrous oxide budgets: moving targets as we enter the anthropocene?, Science Marine, 65, 85–105, 2001. 5513

de Sousa, S. N., Kumar, M. D., Sardessai, S., Sarma, V. V. S. S., and Shirodkar, P. V.: Seasonal variability in oxygen and nutrients in the central and eastern Arabian Sea, Curr. Sci., 71, 847–851, 1996. 5511, 5512, 5528

Diaz, R. J. and Rosenberg, R.: Spreading dead zones and consequences for marine ecosystems, Science, 321, 26–29, 2008. 5513

Dutkiewicz, S., Follows, M. J., and Parekh, P.: Interactions of the iron and phosphorus cycles: A three-dimensional model study, Global Biogeochem. Cy., 19, GB1021, doi:10.1029/2004GB002342, 2005. 5515

Falkowski, P.: Evolution of the nitrogen cycle and its influence on the biological sequestration of CO_2 in the ocean, Nature, 327, 242–244, 1997. 5513

Findlater, J.: A major low-level air current near the Indian Ocean during the northern summer, Q. J. Roy. Meteorol. Soc., 95, 362–380, 1969. 5511

Fischer, A. S., Weller, R. A., Rudnick, D. L., Eriksen, C. C., Lee, C. M., Brink, K. H., Fox, C. A., and Leben, R. R.: Mesoscale eddies, coastal upwelling, and the upper-ocean heat budget in the Arabian Sea, Deep Sea Res. II, 49, 2231–2264, doi:10.1016/S0967-0645(02)00036-X, 2002. 5512, 5529

Flagg, C. and Kim, H.-S.: Upper ocean currents in the northern Arabian Sea from shipboard ADCP measurements during the 1994–1996 U.S. JGOFS and ONR programs, Deep-Sea Res. II, 45, 1917–1960, 1998. 5529

Garrison, D. L., Gowing, M. M., and Hughes, M. P.: Nano- and microplankton in the northern Arabian Sea during the Southwest Monsoon, August-September 1995 A US-JGOFS study, Deep Sea Res. II, 45, 2269–2299, doi:10.1016/S0967-0645(98)00071-X, 1998. 5514

Han, W., McCreary, J. P., masumoto, Y., Vialard, J., and Duncan, B.: Basin modes in the equatorial Indian Ocean, J. Phys. Oceanogr., 41, 1252–1270, 2011. 5522

Hitchcock, G. L., Key, E. L., and Masters, J.: The fate of upwelled waters in the Great Whirl, August 1995, Deep Sea Res. II, 47, 1605–1621, doi:10.1016/S0967-0645(99)00156-3, 2000. 5511

Jaccard, S. L. and Galbraith, E. D.: Large climate-driven changes of oceanic oxygen concentrations during the last deglaciation, Nature Geosci., 5, 151–156, doi:10.1038/ngeo1352, 2012. 5531

Kawamiya, M.: Mechanism of offshore nutrient supply in the western Arabian Sea, J. Marine Res., 59, 675–696, 2001. 5528

Keeling, R. F., Koertzinger, A., and Gruber, N.: Ocean Deoxygenation in a warming world, Annu. Rev. Mar. Sci., 2, 199–229, doi:10.1146/annurev.marine.010908.163855, 2010. 5530, 5531

Keen, T., Kindle, J., and Young, D.: The interaction of Southwest Monsoon upwelling, advection and primary production in the northwest Arabian Sea, J. Marine Syst., 13, 61–82, 1997. 5528

Kim, H.-S., Flagg, C. N., and Howden, S.: Northern Arabian Sea variability from TOPEX/Poseidon altimetry data, An extension of the JGOFS/ONR shipboard ADCP study, Deep-Sea Res. II, 48, 1069–1096, 2001. 5529

Koné, V., Aumont, O., Lévy, M., and Resplandy, L.: Physical and Biogeochemical Controls of the Phytoplankton Seasonal Cycle in the Indian Ocean: a modeling study, in: Indian Ocean Biogeochemical Processes and Ecological Variability, edited by: Wiggert, J. D., Hood, R. R., Naqvi, S. W. A., Brink, K. H., and Smith, S. L., vol. 185, 147–166, American Geophysical Union, Washington DC, USA, 2009. 5515, 5516

Lapeyre, G., Klein, P., and Hua, B.: Oceanic Restratification Forced by Surface Frontogenesis, J. Phys. Oceanogr., 36, 1577–1590, 2006. 5529

Lee, C. M., Jones, B. H., Brink, K. H., and Fischer, A. S.: The upper-ocean response to monsoonal forcing in the Arabian Sea: seasonal and spatial variability, Deep-Sea Res. II, 47, 1177–1226, 2000. 5528

Leth, O. and Middleton, J.: A mechanism for enhanced upwelling off central Chile: Eddy advection, J. Geophys. Res., 109, C12020, doi:10.1029/2003JC002129, 2004. 5528

Levin, L. A., Ekau, W., Gooday, A. J., Jorissen, F., Middelburg, J. J., Naqvi, S. W. A., Neira, C., Rabalais, N. N., and Zhang, J.: Effects of natural and human-induced hypoxia on coastal benthos, Biogeosciences, 6, 2063–2098, doi:10.5194/bg-6-2063-2009, 2009. 5513

Levitus, S., Boyer, T., Conkright, M., O'Brian, T., Antonov, J., Stephens, C., Stathopolos, L., Johnson, D., and Gelfeld, R.: World Ocean database 1998, technical Report NESDID18, NOAA Atlas, 1998. 5514

Lévy, M., Mémery, L., and Madec, G.: The onset of the spring bloom in the MEDOC area: mesoscale spatial variability, Deep Sea Res. I, 46, 1137–1160, doi:10.1016/S0967-0637(98)00105-8, 1999. 5529

Lévy, M., Estubier, A., and Madec, G.: Choice of an advection scheme for biogeochemical models, Geophys. Res. Lett., 28, 3725–3728, 2001. 5516

Lévy, M., Shankar, D., André, J.-M., Shenoi, S. S. C., Durand, F., and de Boyer Montégut, C.: Basin-wide seasonal evolution of the Indian Ocean's phytoplankton blooms, J. Geophys. Res., 112, C12014, doi:10.1029/2007JC004090, 2007. 5511

Lévy, M., Trguier, P. K. A.-M., Iovino, D., Madec, G., Masson, S., and Takahashi, K.: Modifications of gyre circulation by sub-mesoscale physics, Ocean Modell., 34, 1–15, doi:10.1016/j.ocemod.2010.04.001, 2010. 5529

Lierheimer, L. J. and Banse, K.: Seasonal and interannual variability of phytoplankton pigment in the Laccadive (Lakshadweep) Sea as observed by the Coastal Zone Color Scanner, Proc. Ind. Acad. Sci.-Earth and Planet. Sci., 111, 163–185, 2002. 5511

Madec, G.: NEMO, the ocean engine, Note du Pole de modélisation, Institut Pierre-Simon Laplace (IPSL), France, No 27 ISSN No 1288-1619, available at: www.nemo-ocean.eu/About-NEMO/Reference-manuals, 2008. 5514

Madhupratap, S. P. K., Bhattathiri, P. M. A., Kumar, M. D., Raghukumar, S., Nair, K. K. C., and Ramaiah, N.: Mechanism of the biological response to winter cooling in the northern Arabian Sea, Nature, 384, 549–552, 1996. 5511

Manghnani, V., Morrison, J. M., Hopkins, T. S., and Böhm, E.: Advection of upwelled waters in the form of plumes off Oman during the Southwest Monsoon, Deep-Sea Res. II, 45, 2027–2052, 1998. 5528

McCreary, J. P., Hood, R., and Yu, Z.: Modelling the Arabian Sea Oxygen Minimum Zone, Imber Newsletter, 19, www.imber.info, 2011. 5530

Moore, J. K., Doney, S. C., and Lindsay, K.: Upper ocean ecosystem dynamics and iron cycling in a global three-dimensional model, Global Biogeochem. Cy., 18, GB4028, doi:10.1029/2004GB002220, 2004. 5515

Morrison, J. M., Codispoti, L. A., Smith, S. L., Wishner, K., Flagg, C., Gardner, W. D., Gaurin, S., Naqvi, S. W. A., Manghnani, V., Prosperie, L., and Gundersen, J. S.: The oxygen minimum zone in the Arabian Sea during 1995 - overall seasonal and geographic patterns, and relationship to oxygen gradients, Deep Sea Res. II, 46, 1903–1931, doi:10.1016/S0967-0645(99)00048-X, 1999. 5511, 5512

Naqvi, S. W. A., Yoshinari, T. Naik, H., Jayakumar, D. A., Altabet, M. A., Narvekar, P., Devol, A., Brandes, J. A., and Codispoti, L. A.: Budgetary and biogeochemical implications of N_2O isotope signatures in the Arabian Sea, Nature, 394, 462–464, 1998. 5513

Naqvi, S. W. A., Naik, H., Pratihary, A., D'Souza, W., Narvekar, P. V., Jayakumar, D. A., Devol, A. H., Yoshinari, T., and Saino, T.: Coastal versus open-ocean denitrification in the Arabian Sea, Biogeosciences, 3, 621–633, doi:10.5194/bg-3-621-2006, 2006. 5513

Nurser, A. J. G. and Zhang, J. W.: Eddy-induced mixed layer shallowing and mixed layer/thermocline exchange, J. Geophys. Res., 105, 851–868, 2000. 5529

Olson, D. B., Hitchcock, G. L., Fine, R. A., and Warren, B. A.: Maintenance of the low-oxygen layer in the central Arabian Sea, Deep Sea Res. II, 40, 673–685, doi:10.1016/0967-0645(93)90051-N, 1993. 5512

Ono, T., Midorikawa, T., Watanabe, Y. W., Tadokoro, K., and Saino, T.: Temporal increases of phosphate and apparent oxygen utilization in the subsurface waters of western subarctic Pacific from 1968 to 1998, Geophys. Res. Lett., 28, 85–88, 2001. 5531

Oschlies, A.: Improved representation of upper ocean dynamics and mixed layer depths in a model of the North Atlantic on switching from eddy-permitting to eddy-resolving grid resolution, J. Phys. Oceanogr., 32, 2277–2298, 2002. 5529

Paulmier, A. and Ruiz-Pino, D.: Oxygen minimum zones (OMZs) in the modern ocean, Prog. Oceanogr., 80, 113–128, doi:10.1016/j.pocean.2008.08.001, 2009. 5518

Rao, R., Molinari, R., and Festa, J.: Evolution of the Climatological Near-Surface Thermal Structure of the Tropical Indian Ocean 1. Description of Mean Monthly Mixed Layer Depth, and Sea Surface Temperature, Surface Current, and Surface Meteorological Fields, J. Geophys. Res., 94, 10801–10815, 1989. 5512

Resplandy, L., Lévy, M., Madec, G., Pous, S., Aumont, O., and Kumar, D.: Contribution of mesoscale processes to nutrient budgets in the Arabian Sea, J. Geophys. Res., 116, C11007, doi:10.1029/2011JC007006, 2011. 5513, 5516, 5518, 5529

Ryther, J. H. and Menzel, D. W.: On the production, composition, and distribution of organic matter in the Western Arabian Sea, Deep Sea Res. I, 12, 199–209, 1965. 5512

Sarma, V. V. S. S.: An evaluation of physical and biogeochemical processes regulating perennial suboxic conditions in the water column of the Arabian Sea, Global Biogeochem. Cy., 16, 1082, doi:10.1029/2001GB001461, 2002. 5512, 5520, 5527

Schott, F. A. and McCreary, J. P.: The monsoon circulation of the Indian Ocean, Prog. Oceanogr., 51, 1–123, 2001. 5512, 5529, 5540

Severdrup, H., U., Johnson, M. W., and Fleming, R. H.: The Ocean: Their Physics, Chemistry and General Biology, Prentice-Hall, 696 pp., old Tappan, 1942. 5512

Shchepetkin, A. F. and McWilliams, J. C.: The regional oceanic modeling system (ROMS): a split-explicit, free-surface, topography-following-coordinate oceanic model, Ocean Modell., 9, 347–404, doi:10.1016/j.ocemod.2004.08.002, 2005. 5514

Shetye, S. R., Gouveia, A. D., Shenoi, S. S. C., Sundar, D., Michael, G. S., Almeida, A. M., and Santanam, K.: Hydrography and circulation off the West coast of India during the Southwest monsoon 1987, J. Marine Res., 48, 359–378, 1990. 5522

Stramma, L., Johnson, G. C., Sprintall, J., and Mohrholz, V.: Expanding Oxygen-Minimum Zones in the Tropical Oceans, Science, 320, 655–658, doi:10.1126/science.1153847, 2008. 5531

Stramma, L., Prince, E. D., Schmidtko, S., Luo, J., Hoolihan, J. P., Visbeck, M., Wallace, D. W. R., Brandt, P., and Körtzinger, A.: Expansion of oxygen minimum zones may reduce available habitat for tropical pelagic fishes, Nature Climate Change, 2, 33–37, doi:10.1038/nclimate1304, 2011. 5531

Takahashi, T., Broecker, W. S., and Langer, S.: Redfield ratio based on chemical data from isopycnal surfaces, J. Geophys. Res., 90, 6907–6924, 1985. 5515

Treguier, A., Barnier, B., de Miranda, A., Molines, J. M., Grima, N., Imbard, M., Madec, G., Messager, C., Reynaud, T., and Michel, S.: An eddy-permitting model of the Atlantic circulation: Evaluating open boundary conditions, J. Geophys. Res., 106, 22115–22129, 2001. 5514

Van Leer, B.: Towards the Ultimate Conservative Difference Scheme, V. a Second Order Sequel to Godunov's Method, Journal of Computational Physics, 32, 101–136, 1979. 5516

Veldhuis, M. J. W., Kraay, G. W., Bleijswijk, J. D. L. V., and Baars, M. A.: Seasonal and spatial variability in phytoplankton biomass, productivity and growth in the northwestern Indian Ocean: the Southwest and Northeast Monsoon, 1992–1993, Deep Sea Res. I, 44, 425–449, doi:10.1016/S0967-0637(96)00116-1, 1997. 5511

Weller, R. A., Fischer, A. S., Rudnick, D. L., Eriksen, C. C., Dickey, T. D., Marra, J., Fox, C., and Leben, R.: Moored observations of upper-ocean response to the monsoons in the Arabian Sea during 1994–1995, Deep Sea Res. II, 49, 2195–2230, doi:10.1016/S0967-0645(02)00035-8, 2002. 5511, 5512

Wiggert, J. D., Hood, R., Banse, K., and Kindle, J.: Monsoon-driven biogeochemical processes in the Arabian Sea, Prog. Oceanogr., 65, 176–213, doi:10.1016/j.pocean.2005.03.008, 2005. 5511

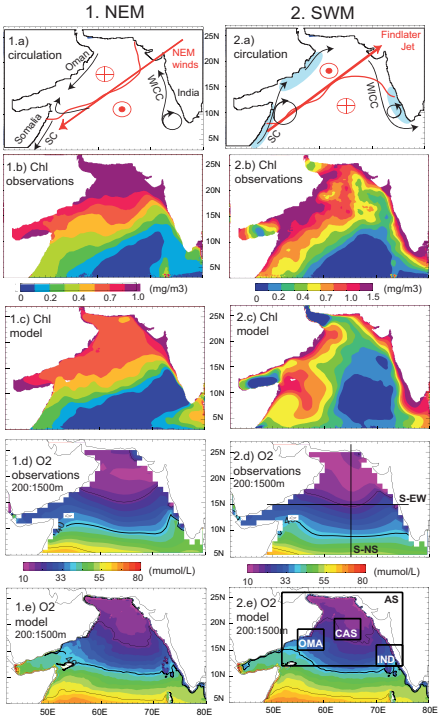

Fig. 1. Climatological maps during the **(1)** northeast monsoon (NEM) and **(2)** southeast monsoon (SWM): **(a)** Schematic representation of dominant winds (red arrows), oceanic circulation (black arrows), coastal upwelling systems (blue shading) and Ekman pumping (red symbol) adapted from Schott and McCreary (2001). The reversing Somali Current (SC) and Western Indian Coastal Current (WICC) are indicated; **(b, c)** surface chlorophyll (Chl, in mg m^{-3}) climatology from satellite SeaWiFS (1998–2005) **(b)** and simulated in the model **(c)**; **(d–e)** oxygen concentration averaged between 200 and 1500 m in WOA09 **(d)** and simulated in the model **(e)**. Sections S-EW and S-NS presented on Fig. 3 and Fig. 4 are indicated on **(2.d)**. Regions AS, CAS, OMA and IND are indicated on **(2.e)**.

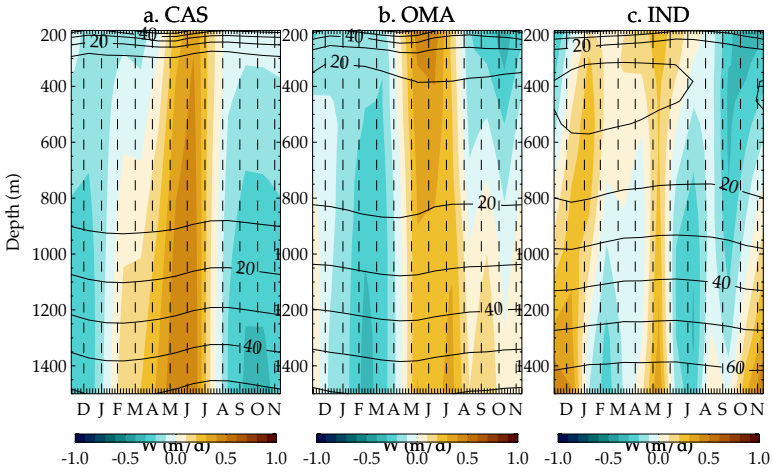

Fig. 2. Simulated vertical velocities between 200 and 1500 m in **(a)** CAS, **(b)** OMA and **(c)** IND regions (see Fig. 1(2.e)). Units are in m d^{-1}. Contours indicate the oxygen concentration in the region.

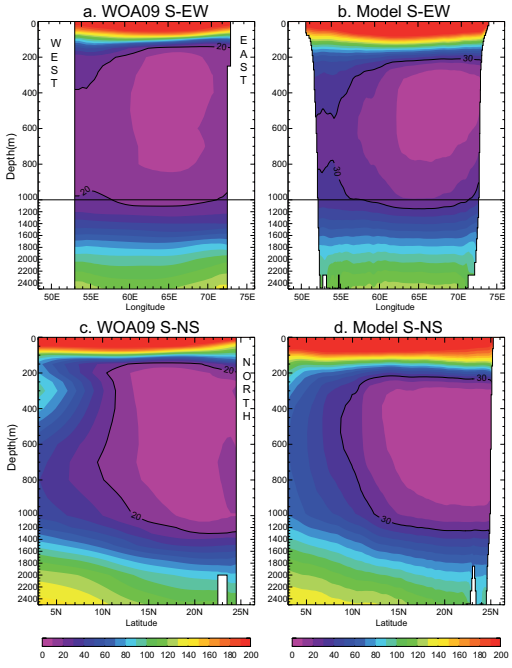

Fig. 3. Annual oxygen concentration (in µmol l^{-1}) along the east-west (S-EW) and north-south (S-NS) sections indicated on Fig. 1(2.d) in: **(a)** WOA09 climatology and **(b)** the model.

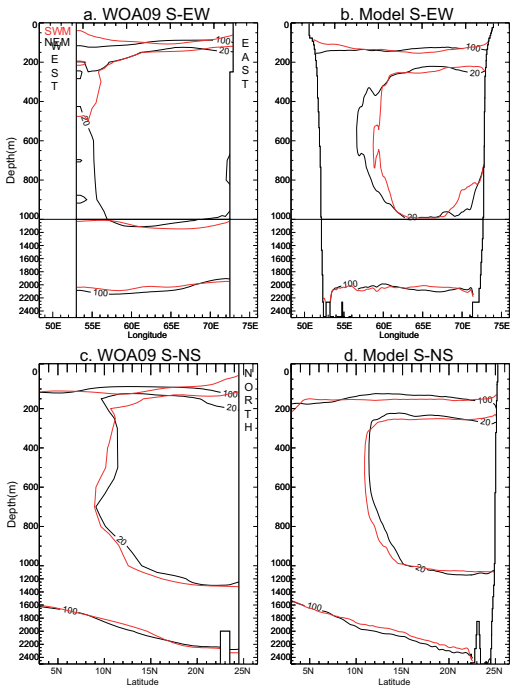

Fig. 4. Seasonal variability of the OMZ's core (20 µmol l^{-1} contour) and of the 100 µmol l^{-1} isoline along the east-west (S-EW) and north-south (S-NS) sections indicated on Fig. 1(2.d). Contours are given for the winter (NEM in black) and summer (SWM in red) monsoons in: **(a, c)** WOA09 climatology and **(b, d)** the model.

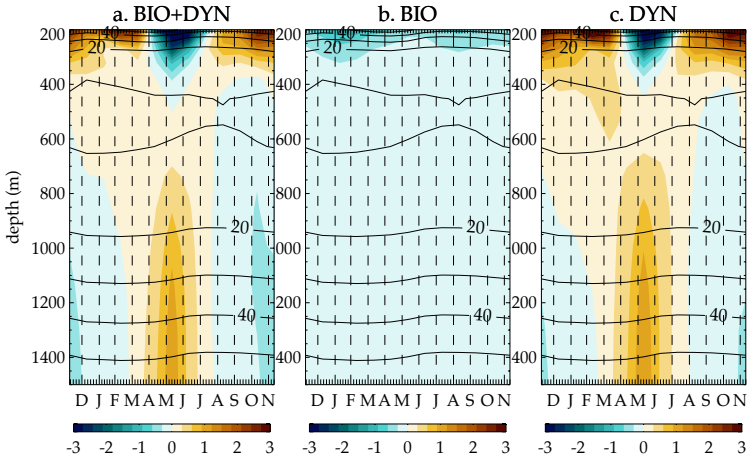

Fig. 5. Simulated seasonal trends of oxygen averaged between 200 and 1500 m in the AS region (see Fig. 1(2.e)): **(a)** sum of biological and dynamical terms, **(b)** biological terms and **(c)** dynamical terms. Units are in µmol l^{-1} $month^{-1}$. Contours indicate the oxygen concentration in the region.

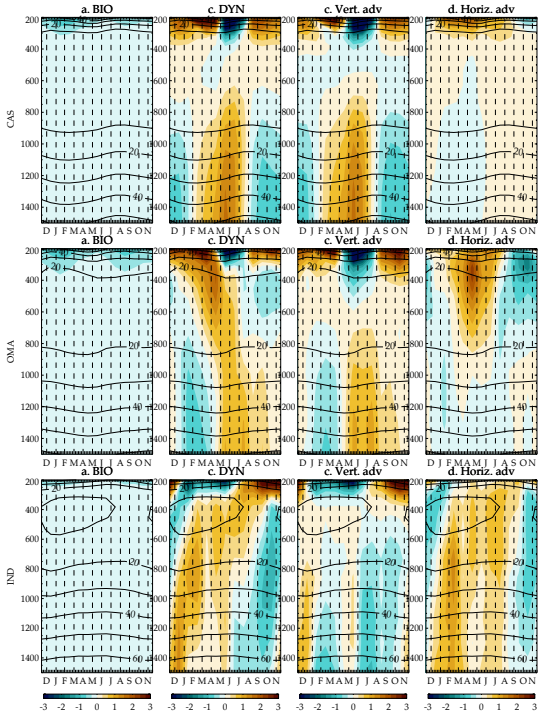

Fig. 6. Simulated seasonal trends of oxygen between 200 and 1500 m in the CAS, OMA and IND regions (see Fig. 1(2.e)): **(a)** biological terms, **(b)** dynamical terms, **(c)** vertical advection and **(d)** horizontal advection. Units are in $\mu mol\,l^{-1}\,month^{-1}$. Contours indicate the oxygen concentration in the region.

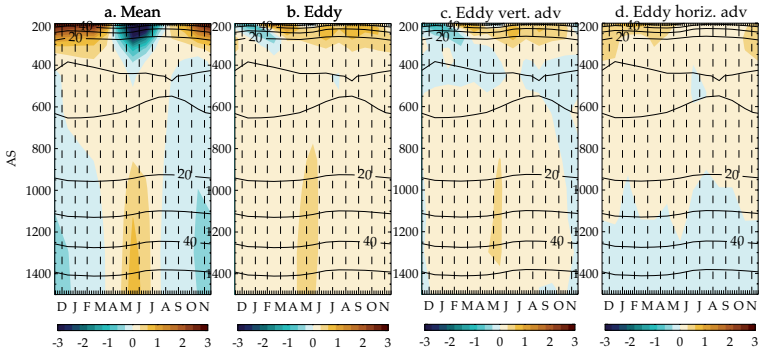

Fig. 7. Simulated seasonal trends of oxygen between the 200 and 1500 m in the AS region (see Fig. 1(2.e)): **(a)** mean transport, **(b)** eddy-driven transport, **(c)** eddy-driven vertical transport and **(d)** eddy-driven lateral transport. Units are in $\mu mol\,l^{-1}\,month^{-1}$. Contours indicate the oxygen concentration in the region.

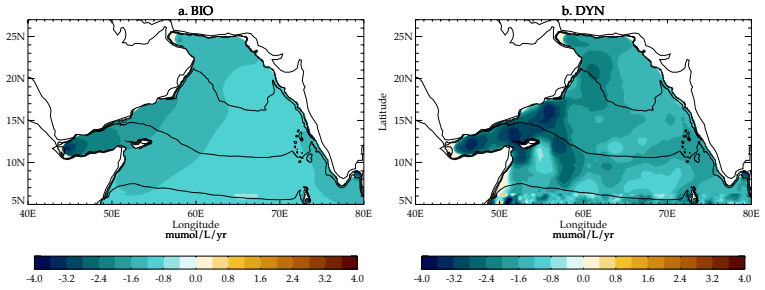

Fig. 8. Annual mean of the simulated trends of oxygen averaged between the 200 and 1500 m: **(a)** biological terms ($\left(\frac{\partial O_2}{\partial t}\right)_{Bio}$), **(b)** minus dynamical terms ($-\left(\frac{\partial O_2}{\partial t}\right)_{Dyn}$). Refer to Eq. (2). Units are in $\mu mol\, l^{-1}\, yr^{-1}$.

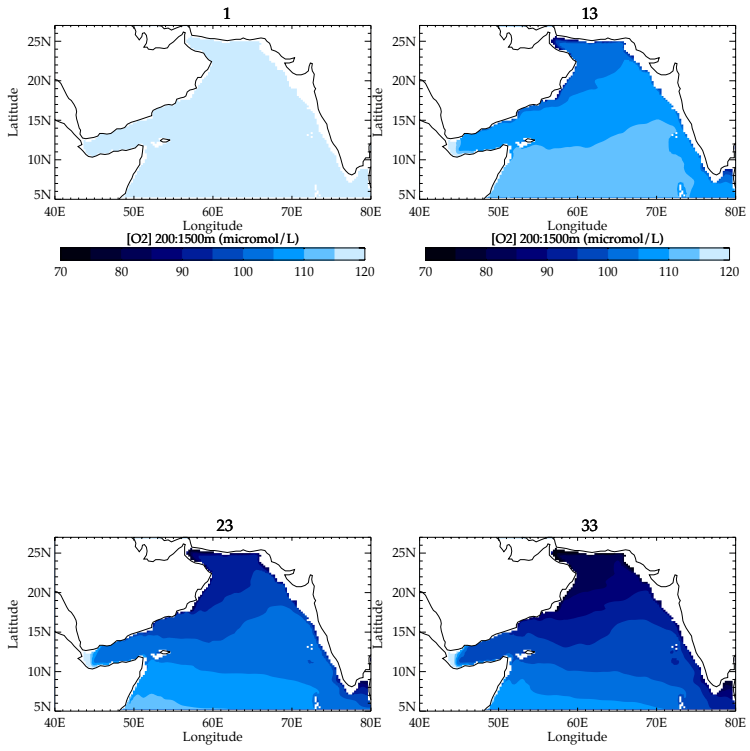

Fig. 9. Simulated OMZ formation: oxygen concentration averaged at the OMZ depth (between 100 and 1000 m) in the simulation initialized with no OMZ after 1, 13, 23 and 33 yr of simulation.

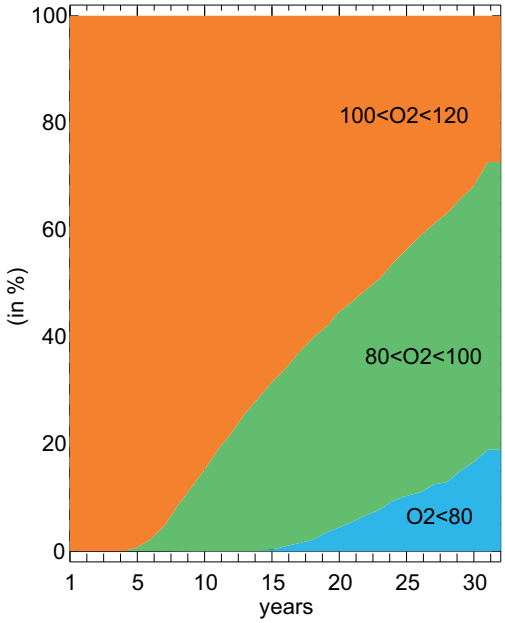

Fig. 10. OMZ formation: temporal evolution of waters with oxygen concentrations between 100 and 120 µmol l^{-1}, between 80 and 100 µmol l^{-1} and below 80 µmol l^{-1} during the 33 yr of simulation (in % of the total volume).

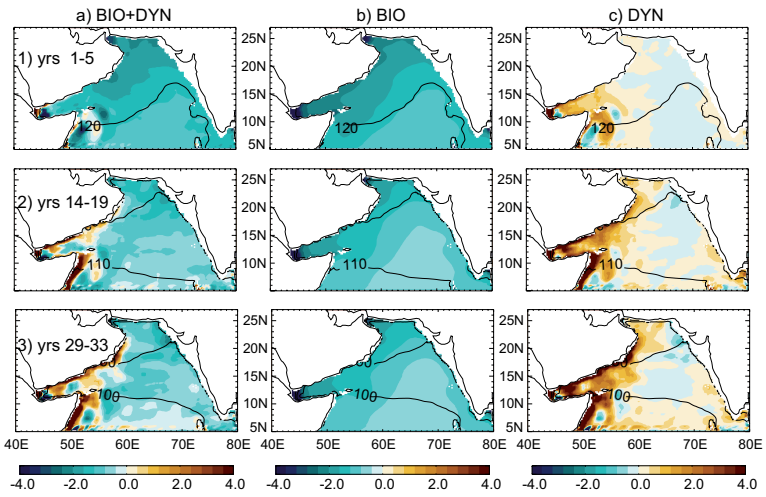

Fig. 11. OMZ formation: averaged simulated trends of oxygen averaged between 200 and 1500 m for three different periods of the simulation. **(1)** years 1 to 5, **(2)** years 14 to 18 and **(3)** years 29 to 33. Contours indicate the mean oxygen concentration between 200 and 1500 m during each period.